On the Link Between Contaminant Source Release Conditions and Plume Prediction Uncertainty

Felipe P. J. de Barros

Institute for Applied Analysis and Numerical Simulation/SRC SimTech, Pfaffenwaldring 57, University of Stuttgart, 70569 Stuttgart, Germany

Wolfgang Nowak

Institute of Hydraulic Engineering (LH^2)/ SRC SimTech, Pfaffenwaldring 61, University of Stuttgart, 70569 Stuttgart, Germany

Abstract

The initial width of contaminant plumes is known to have a key influence on expected plume development, dispersion and travel time statistics. In past studies, initial plume width has been perceived identical to the geometric width of a contaminant source or injection volume. A recent study on optimal sampling layouts (Nowak et al., 2010) showed that a significant portion of uncertainty in predicting plume migration stems from the uncertain total hydraulic flux through the source area. This result points towards a missing link between source geometry and plume statistics, which we denote as the effective source width. We define the *effective* source width by the ratio between the actual and expected hydraulic flux times the *geometric* source width. The actual hydraulic flux through the source area is given by individual realizations while the expected one represents the mean over the ensemble. It is a stochastic quantity that may strongly differ from the actual geometric source width for geometrically small sources, and becomes identical only at the limit of wide sources (approaching ergodicity). We derive its stochastic ensemble moments in order to explore the dependency on source scale. We show that, if the effective source width is known rather than the geometric width, predictions of plume development can greatly increase in predictive power. This is illustrated on plume statistics such as the distribution of plume length, average width, transverse dispersion, total mass flux and overall concentration variance. The analysis is limited to 2D depth-averaged systems, but implications hold for 3D cases.

Keywords: Stochastic Hydrogeology, Heterogeneous porous media, Stream function statistics, Contaminant dispersion, Conditioning

1. Introduction

Stochastic description of contaminant transport is a necessity since full characterization of natural porous media, such as aquifers, is an unfeasible task. Many past studies have provided powerful tools to predict contaminant transport, based on the ensemble behavior of the plume's spatial and temporal moments (for an extensive review see Rubin, 2003). In these studies, the initial width of a plume (e.g., the dimension of the contaminant source) is directly related to fundamental characteristics such as plume ergodicity and is a key parameter in predictions of plume development, dispersion, dilution and mixing (e.g., Rubin et al., 1994; Andricevic and Cvetkovic, 1998; Dentz et al., 2000).

Up to date, the initial plume width has been perceived as identical to the width of a source or of an injection volume (e.g., Dentz et al., 2000; Fiorotto and Caroni, 2002; Schwede et al., 2008). A recent study by Nowak et al. (2010) has identified optimal sampling strategies for minimum variance prediction of contaminant concentrations at environmentally sensitive locations located downgradient of the source. In their resulting optimal designs, the largest number of samples is spent in order to investigate certain hydraulic phenomena directly at the source location rather than transport phenomena further down-gradient. The authors proposed that the major source of uncertainty addressed by these optimal sampling schemes is the total volumetric water flux passing through the source area.

The importance of focused volumetric water flux in the spreading of contaminants in saturated porous media is shown in Werth et al. (2006) and Valocchi and Nakshatrala (2009). These authors showed, through numerical and analytical approaches, how the convergence of streamlines within some given zone can enhance the transverse mixing of the plume. When flow is focused within a high permeability zone, streamlines converge and then diverge again. While the streamlines are closer together, a higher diffusive transfer of solute mass is faciliated, contributing to lateral plume dilution. The opposite occurs when flow is blocked by a low-permeability zone. Experimental evidence was also shown in Rahman et al. (2005) and recently by Rolle et al. (2009), where the squeezing of contaminant plumes in high permeability inclusions was investigated. Based on their experimental observations, Rahman et al. (2005) defined a source equivalent width which is a function of the volumetric injection rate (in similar fashion to the asymptotic catchment zone width of a pumping well which is defined by the ratio between background flow and pumping rate). Recently, Valocchi and Nakshatrala (2009) showed the sensitivity of transversal spreading on the contaminant source location. They illustrated how spreading is enhanced if the source is located within high- or low-permeability zones. In this paper, we will show that the effects of streamline convergence/divergence are much more relevant if it occurs at the contaminant source location, because it influences the entire transport regime (mass flux, plume width, etc.) farther downstream. Strong field evidence for the relevance of local field hydraulic conditions at the source zone my be found in Frind et al. (1999), where the plume leaving a DNAPL source was unexpectedly thin and could almost not be detected.

The above evidence and discussion indicates that there is a missing link between a given source geometry and the resulting width of a plume. The basic idea of the current work is to differentiate between the actual geometric width of the source zone and its effective width, related by what we denote as the source efficiency. We define source efficiency as the ratio of actual (in each realization) versus the expected (ensemble mean) hydraulic flux passing through the geometric area of the source. In real situations, the actual hydraulic flux through the source can be obtained by collecting head and hydraulic conductivity measurements around the source area. Consequently, this data could be used to condition simulations, see Ch. 3 of Rubin (2003). The effective source width is an uncertain quantity that results from the stochastic nature of total discharge through the cross-sectional area where the contaminant source is located. Hence, its theoretical statistical moments can be derived from the integral statistics of specific discharge within the source volume.

The results by Nowak et al. (2010) indicate that effective source width is a key parameter in the prediction of contaminant transport. In their work on concentration probability functions, Schwede et al. (2008) conceptualized the uncertainty of flow rate in the source, but approximated it by point-scale velocity statistics. However, velocity at a single point has different statistics than the integral discharge over the cross-sectional area of a non-point source. Hence, further efforts are necessary to investigate the properties of source hydraulics. We hypothesize that, if the effective source width at a given site was known, predictions of contaminant plume development (i.e., total mass flux, plume length, width, dispersion, dilution and concentration variance) would increase in predictive power. The aim of the current work is to support this hypothesis through the use of closed-formed analytical expressions for effective source width derived from the governing equations of flow. We verify its validity with high-resolution numerical Monte-Carlo flow and transport simulations of characteristic plume statistics depending on the effective source width in a 2D depth-averaged setting.

Section 2 introduces the concept of effective source width along with its mathematical formulation. We also define a parameter denoted source efficiency η, which according to our definition, absorbs all randomness of effective source width. Section 3 derives of the statistical moments of source efficiency. The effects, significance and implications of the results with respect to plume prediction and its spatial moments are illustrated in Section 4. Finally, conclusions are given in Section 5.

2. The Concept of Effective Source Width

2.1. Mathematical Formulation

In the following, we will differentiate between the geometric width of the source zone (w_{sz}) and its effective width (w_{eff}). We consider an incompressible, fully saturated, two-dimensional steady-state flow within a confined, depth-averaged aquifer. Let $\mathbf{x} = (x_1, x_2)$ represent the cartesian coordinate system with velocity field $\mathbf{v}$ satisfying Darcy's Law. The mean flow is taken along the direction x_1. Consider a contaminant line source (width equal to w_{sz}) perpendicular to the direction of mean flow with fixed concentration c_o (other release conditions are discussed in Section 4.5). The effective source width, w_{eff}, is defined with the aid of the continuity equation:

$$w_{eff} = w_{sz} \frac{Q_{sz}}{\langle Q_{sz} \rangle}, \tag{1}$$

where Q_{sz} is the volumetric water flux passing through the source zone:

$$Q_{sz} = \int\limits_{w_{sz}} q_1(x_1, x_2) b dx_2 \,. \tag{2}$$

Here, b denotes aquifer depth, $q_1\,(x_1, x_2)$ the specific discharge passing through the source zone and $\langle \cdot \rangle$ the ensemble expectation. Taking the geometric source width as a given quantity in equation (1), the randomness lies in the source efficiency denoted as η:

$$\eta = \frac{Q_{sz}}{\langle Q_{sz} \rangle} \,. \tag{3}$$

For an unbounded two-dimensional aquifer with uniform-in-the-average flow, $\langle Q_{sz} \rangle$ is given by:

$$\langle Q_{sz} \rangle = J T_G w_{sz} \,, \tag{4}$$

where J is the mean hydraulic gradient in the x_1 direction and T_G is the geometric mean of transmissivity. Equation (4) applies because T_G is the effective transmissivity for infinite, two-dimensional aquifers (for a quick reference, see Ch. 5 of Rubin, 2003). In addition, we can express Q_{sz} in terms of the stream function values that bound the edges of the geometrical source (namely, ψ_s and ψ_i, see Bear, 1972). The subscripts "s" and "i" corresponds to the superior and inferior streamlines bounding the contaminant source area. The relationship between the Darcy flux and stream function can be found in Bear (1972) and is reproduced for completeness in Appendix A. Now we can re-write equation (3) as follows:

$$\eta = \frac{\psi_s - \psi_i}{J T_G w_{sz}} \,. \tag{5}$$

The stochastic moments of η will follow in section 3 as well as its verification with Monte-Carlo simulations.

2.2. Illustrative Example

In order to establish the importance of source efficiency for predicting contaminant concentrations, we first demonstrate, visually, its general impact on transport problems by performing a Monte-Carlo transport analysis with 20,000 realizations. The physical-mathematical formulation, boundary conditions and numerical implementation details are provided in Appendix A with parameter values given in Table 1. For each realization, we computed the total volumetric flux passing through the source zone to obtain the respective source efficiency η and the effective source width w_{eff}. From that ensemble, we extracted two subsets, one with effective source width $w_{eff} > 3/2\, w_{sz}$ and another with $w_{eff} < 1/2\, w_{sz}$ (in terms of source efficiency: η >3/2 or η >1/2). The respective concentration mean and variance fields of the total Monte Carlo set and extracted subsets are shown in Figures 1.a-c and 2.a-c.

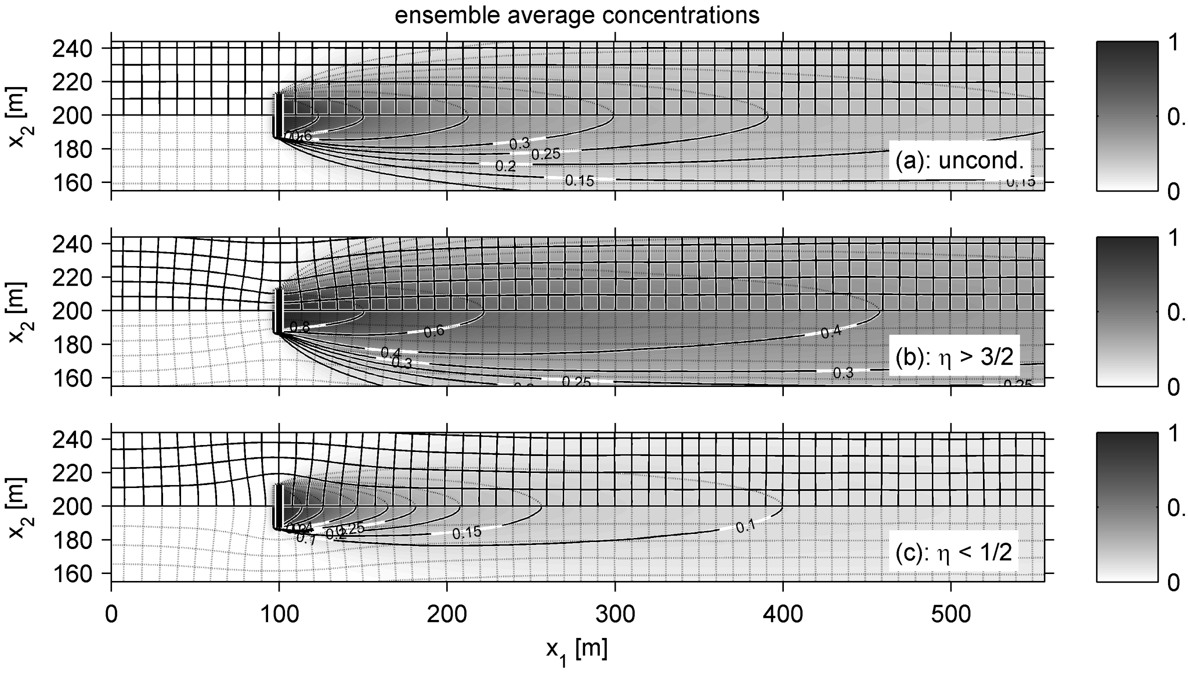

Figure 1: Impact of effective source width, see equations (1) and (3), on ensemble mean concentration (base case scenario). Simulation results for an isotropic exponential covariance model and parameters summarized in Table 1: (a) Concentration mean of the unconditional simulation. (b) Concentration mean of all realizations with source efficiency larger than 3/2. (c) Same for source efficiency smaller than 1/2. For parameter values, refer to Table 1. The black bar in the figure denotes the contaminant source. Contours in the upper half represents streamlines. Contours in the lower half represents isolines of mean concentration.

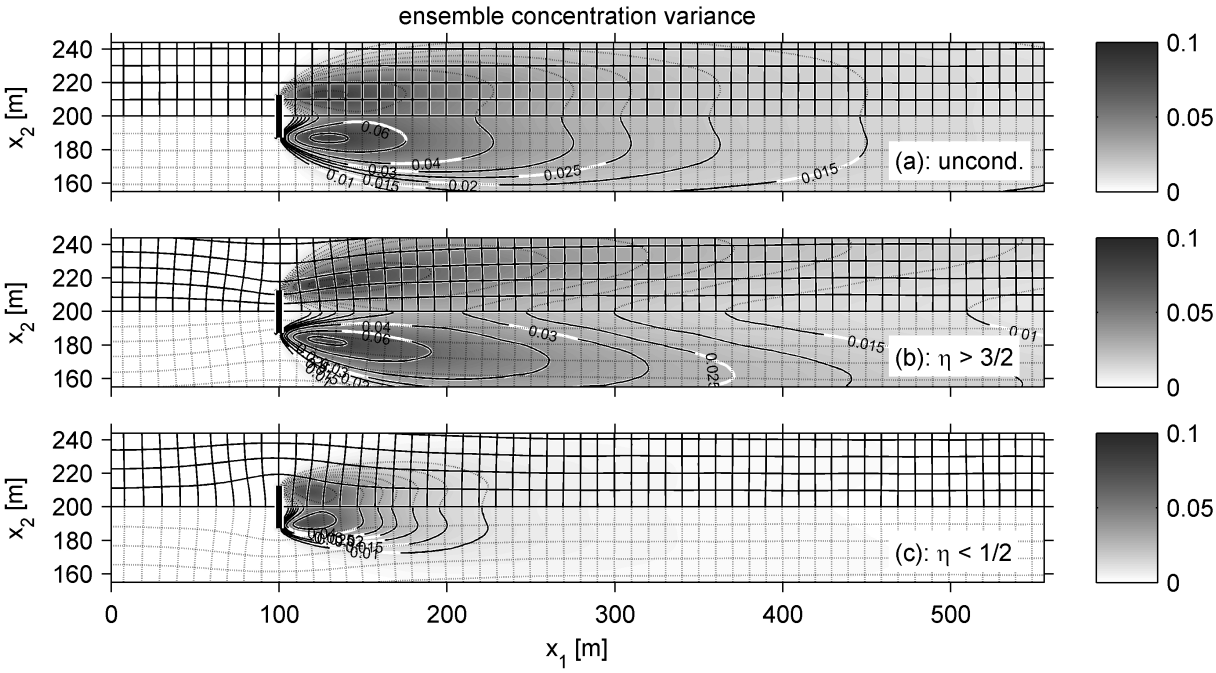

Figure 2: Same as in Figure 1 but for concentration variance. For parameter values, refer to Table 1.

Parameters Used in Simulation	
Domain Size $L \times W$	2500 m×400 m
Grid Size:$(\Delta x_1, \Delta x_2)$	(2, 0.5)
Dispersivities: $(\alpha_{11}, \alpha_{22})$	(2.5, 0.25)
Geostatistical Correlation Length: λ	10 m
Variance of Y: σ_Y^2	2
Geometric Mean for Conductivity: K	0.0004 m/s
Head Gradient: ∇h	0.0008
Source Width: w_{sz}	25 m
Molecular Diffusion: D_m	10^{-9} m^2/s
Geostatistical Covariance Function C_Y	Isotropic Exponential
Effective Porosity n_e	0.35

Table 1: Parameter values used in simulation

The concentration mean of the unfiltered ensemble, as shown in Figure 1.a, follows the classical macro-dispersive transport equation with travel-time dependent dispersion coefficients (e.g., Gelhar and Axness, 1983; Dagan, 1988). The result in Figure 1.b depicts the statistics with sources situated in areas of high volumetric flow rate. It illustrates the mean of all realizations that have an effective source width of $w_{eff} > 3/2\, w_{sz}$ (or $\eta > 3/2$). On average, the realizations with $w_{eff} > 3/2\, w_{sz}$, as shown in Figure 1.b, have a higher transmissivity in the source zone than the global mean. Before passing through the source zone, the streamlines are squeezed, to diverge again downstream of the source. Hence, the average plume is wider than would be expected from the geometric source width regardless of source efficiency, see Figure 1.a. Sources placed within high-volumetric flux zones will emit a larger total contaminant flux $\dot{m}$. This is because, in the advection-dominated case, the total mass flux is directly proportional to the total volumetric flux through the source:

$$\dot{m} = c_o\, Q_{sz}. \tag{6}$$

In addition, known from previous studies, a wider plume is less prone to ensemble dispersion (for a review on this matter, see Rubin, 2003), since the uncertainty in transverse position relates to the plume width. It is also less prone to dilution of the peak concentration along the centerline, since transverse effective dispersion (Dentz et al., 2000) takes more time to reach and diminish the peak concentration at the plume's center. Combined, this leads to an overall longer persistence of high concentrations along the plume's centerline in Figure 1.b.

The opposite case is illustrated in Figure 1.c ($w_{eff} < 1/2\, w_{sz}$ or $\eta < 1/2$): In this case, the resulting plumes are more narrow on-the-average, are more affected by ensemble dispersion and dilution, emits a smaller total flux and are shorter on average. Given this illustrative example, we conclude that effective source width is a singular and highly significant parameter that controls (1) actual plume width, (2) contaminant dispersion and dilution, (3) the total mass flux leaving the source and (4) plume length.

Figure 2 depicts the concentration variance field for the unconditional and conditional simulations. The results show how the behavior of the streamlines at the source location also affect the bimodal characteristics of the concentration variance: Source efficiency influences the magnitude and persistence of the two peaks of high concentration variance at the fringe of the plume throughout the domain. This characteristic of the concentration variance at the plume's fringes (especially at early travel distance) is of importance when quantifying uncertainty in transport (and risk assessment) and has been subject of study in the past (see works by Rubin, 1991; Kapoor and Kitanidis, 1997; Fiori and Dagan, 2000; Fiorotto and Caroni, 2002) and recently by Dentz et al. (2009b) and Dentz et al. (2009a). More details of the Monte Carlo analysis are shown and discussed in subsequent sections.

3. Stochastic Moments of Source Efficiency

3.1. Analytical Development

From equation (5), the source efficiency η results from the stochastic nature of total discharge Q_{sz} (defined in terms of the bounding stream function values) through a finite cross-sectional area of extent w_{sz} perpendicular to the mean flow.

In two-dimensional (depth-averaged) aquifers, the statistics of the bounding stream function values offer a mathematically straightforward way to obtain analytical first-order approximations to the first and second stochastic moment of effective source width. As shown in Appendix B, the mathematical development is straightforward, since well-known methods used for the stochastic groundwater flow equation can be transferred to the corresponding streamline equation.

Since w_{eff} is proportional to η, we now focus on the stochastic moments of η. We start by taking the expected value of η:

$$\langle \eta \rangle = \left\langle \frac{Q_{sz}}{J T_G w_{sz}} \right\rangle = 1. \tag{7}$$

It follows that, of course, the geometric source width is the best estimate of initial plume width in absence of site-specific data. The variance of η is expressed as:

$$\begin{aligned} \sigma_\eta^2 &= \frac{1}{J^2 T_G^2 W_{sz}^2} Var\left[\psi_s - \psi_i\right] \\ &= \frac{2}{J^2 T_G^2 w_{sz}^2} \Gamma_{\psi_s \psi_i}\,, \end{aligned} \tag{8}$$

where $\Gamma_{\psi_s \psi_i}$ is the stream function variogram value for the bounding values ψ_s and ψ_i. The stream function variogram $\Gamma_{\psi_s \psi_i}$ is evaluated at the longitudinal and transversal lag-distances r_1 and r_2 such that $\Gamma_{\psi_s\psi_i} \equiv \Gamma_\psi(0, w_{sz})$. A formal derivation for the stream function variogram, along with the necessary assumptions that includes statistical and temporal stationarity, is given in Appendix B and leads to:

$$\Gamma_\psi\left(r_1,\, r_2\right) = T_G^2 \Gamma_h\left(r_2,\, r_1\right), \tag{9}$$

where Γ_h correponds to the hydraulic head variogram. Equation (9) reflects a rotation of Γ_h by ninety degrees with a scaling factor given by T_G^2. For the given lag distances (dictated by w_{sz}), this leads to:

$$\sigma_\eta^2 = \frac{2}{J^2 w_{sz}^2} \Gamma_h(w_{sz}, 0)\,. \tag{10}$$

After replacing Γ_ψ by the head variogram Γ_h, we can draw on existing analytical solutions. In our case, we will use (for demonstration) the first-order approximation given by Dagan (1985a, 1989), derived for the isotropic exponential covariance model. Figure (3) illustrates how the variance of η decays with increasing values of w_{sz}. Equation (10) quantifies to what degree small sources are more affected by the uncertainty in w_{eff} than wide sources. It indicates the transition to ergodic hydraulic conditions within the source cross-sectional area (rather than ergodic plume width), where effective and geometric source width become almost identical (when the variance becomes negligible), to be around 100 transverse integral scales.

3.2. Verification by Monte-Carlo Simulation

Dagan (1985a) found that first-order approximations for hydraulic head covariances are quite accurate even for higher variances of log-conductivity σ_Y^2. Since our solution is based on the head variogram, we also expect it to be robust even for high values of σ_Y^2. For comparison and verification purposes, we performed an accompanying numerical evaluation by Monte-Carlo analysis of the streamline equation. The results are taken from 20,000 realizations in a domain sized $100\lambda \times 100\lambda$, at a grid spacing of 10 elements per λ, thus easily satisfying the requirement given by Bellin et al. (1992) and Rubin et al. (1999) to adequately resolve heterogeneity on numerical grids. Results were obtained for different values of σ_Y^2 in order to detect the range of vailidity in σ_Y^2. The volumetric fluxes were evaluated at hypothetical source zones with varying width, placed in the center of the domain to minimize boundary influences.

The numerical results are included in Figure 3 as a gray-scale series of lines. The agreement between the analytical and numerical curves for the limiting case of $\sigma_Y^2 \to 0$ is perfect ($\sigma_Y^2 = 0.0001$, results not shown here). Overall, the analytical solution is very robust even at values of $\sigma_Y^2 > 1$. The deviations with increasing σ_Y^2 are conform with recent head and velocity statistics published in the literature: A higher variance of η for small geometrical width coincides with the fact that the local variance of specific discharge scales more than linearly with σ_Y^2 (e.g., Englert et al., 2006; Nowak et al., 2008). Englert et al. (2006) demonstrated that the transverse correlation of specific discharge degenerates with increasing variance of conductivity. This effect explains why the high variance curves again approach our analytical solution with increasing geometric source width. The sudden drop to zero close to 100 integral scales is an artifact of the bounded numerical domain used in our Monte-Carlo analysis. The analytical result for the variance of source efficiency reaches an asymptotic value of zero only for $w_{sz} \to \infty$.

The results in Figure 3 lead to another fundamental question: Over what range of source width does the source efficiency remain the dominant explanatory variable for solute transport prediction? In other words: Over what range of w_{sz} does η display correlation with downstream plume characteristics? Similar to the ergodicity of large domains for the effective flow problem, we expect its impact to fade with increasing geometric width of the source. This question will be pursued in Section 4.3.

3.3. Empirical Probability Density Function for η

In absence of higher-order moments, the maximum entropy assumption would be that η follows a Gaussian distribution (Jaynes, 1982; Singh, 1997). This contradicts with the fact that source efficiency should mostly be non-negative for physical reasons: Negativity would occur only if flow is reversed due to high contrasts in Y (see Englert et al., 2006; Nowak et al., 2008). Therefore, a Gaussian distribution can only be assumed for small variances, where the lower bound at $\eta = 0$ does not yet have a significant influence on the shape of the distribution. The suggestive distribution for η at hand is the log-normal one, accounting for non-negativity. From the above Monte-Carlo analysis for $\sigma_Y^2 = 1$, we evaluated an empirical probability density function (PDF) using a Gaussian Kernel estimate technique with Kernel width equal to 2.56×10^{-4} (Parzen, 1962; Wasserman, 2004). At the same time, we used our analytical first-order results for the mean and variance of η and fitted a log-normal distribution to these two moments. Figure 4 shows good visual

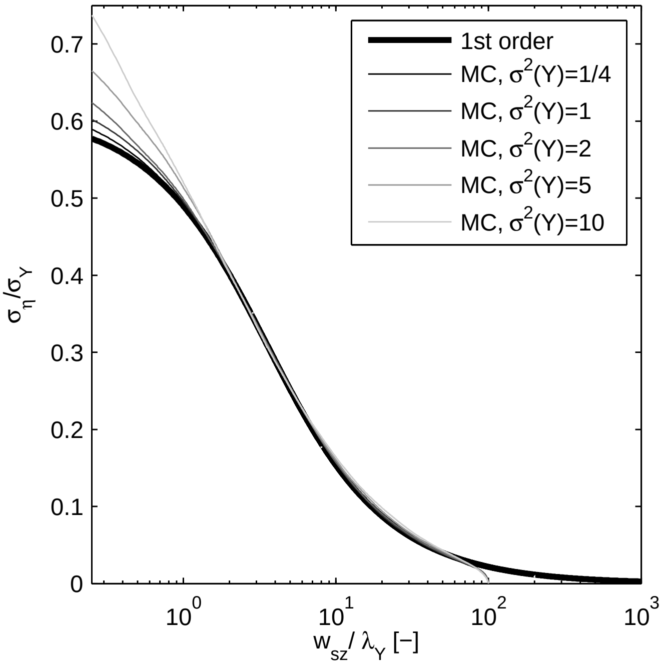

Figure 3: Dependence of source efficiency standard deviation on normalized geometric source width, comparison of analytical first-order expression and results from Monte-Carlo analysis. For parameter values, refer to Table 1.

agreement between the two. For quantitative analysis, we also computed the empirical cumulative distribution function (CDF) from the same Monte-Carlo analysis and evaluated the difference between the empirical CDF and the moment-based log-normal CDF obtained by moment-matching with our analytical first-order moments. The typical maximum difference, measured as in a Kolmogorov-Smirnov test, is in the order of 5%. When repeating the same analysis with a log-normal CDF fitted to the moments obtained from the Monte-Carlo analysis, the maximum difference is in the order of 2% over the entire range of w_{sz}. In conclusion, we recommend to approximate η as a log-normal quantity.

4. Effects, Significance and Implications

4.1. Relation to Plume Length

In many practical applications, hydrogeologists are interested in predicting the extension of a given contamination in order to meet with environmental regulations, for instance risk assessment. In this subsection, we wish to illustrate how source efficiency can be used to better estimate the extent of a concentration isoline as a measure for plume length (denoted by L_P). Figure 5 shows the dependency of L_P on η for different dimensionless concentrations (c/c_o= 0.1, 0.2, 0.4 and 0.8) as a scatter plot. Results were obtained from the Monte-Carlo simulation presented in Section 2.2.

By fixing a value for η, we can predict the length of the plume defined by a given isoline (for example, c/c_o= 0.1). Larger values of η imply a larger extent of the plume (as already shown in Figure 1). The results shown here are limited to a steady-state release condition. However, with increased computional power, one may obtain similar plots for the transient regime. We observe that all fitted curves have the same slope of 2 in log-log scale, implying a quadratic law. In order to make this point clear, consider an idealized situation, similar to the phyisical scenario used to obtain Figure 5, of a steady-state release within a 2D setting with uniform longitudinal velocity U and transversal dispersion D_{22}. Recalling the analytical solution from Domenico and Palciauskas (1982) (which neglects longitudinal dispersion D_{11}) and substituting the effective source width *in lieu* of the actual geometrical source width we have:

$$\frac{c}{c_o} = \mathrm{erf}\left[\frac{\eta\, w_{sz}}{\sqrt{\frac{x}{U} D_{22}}}\right]. \tag{11}$$

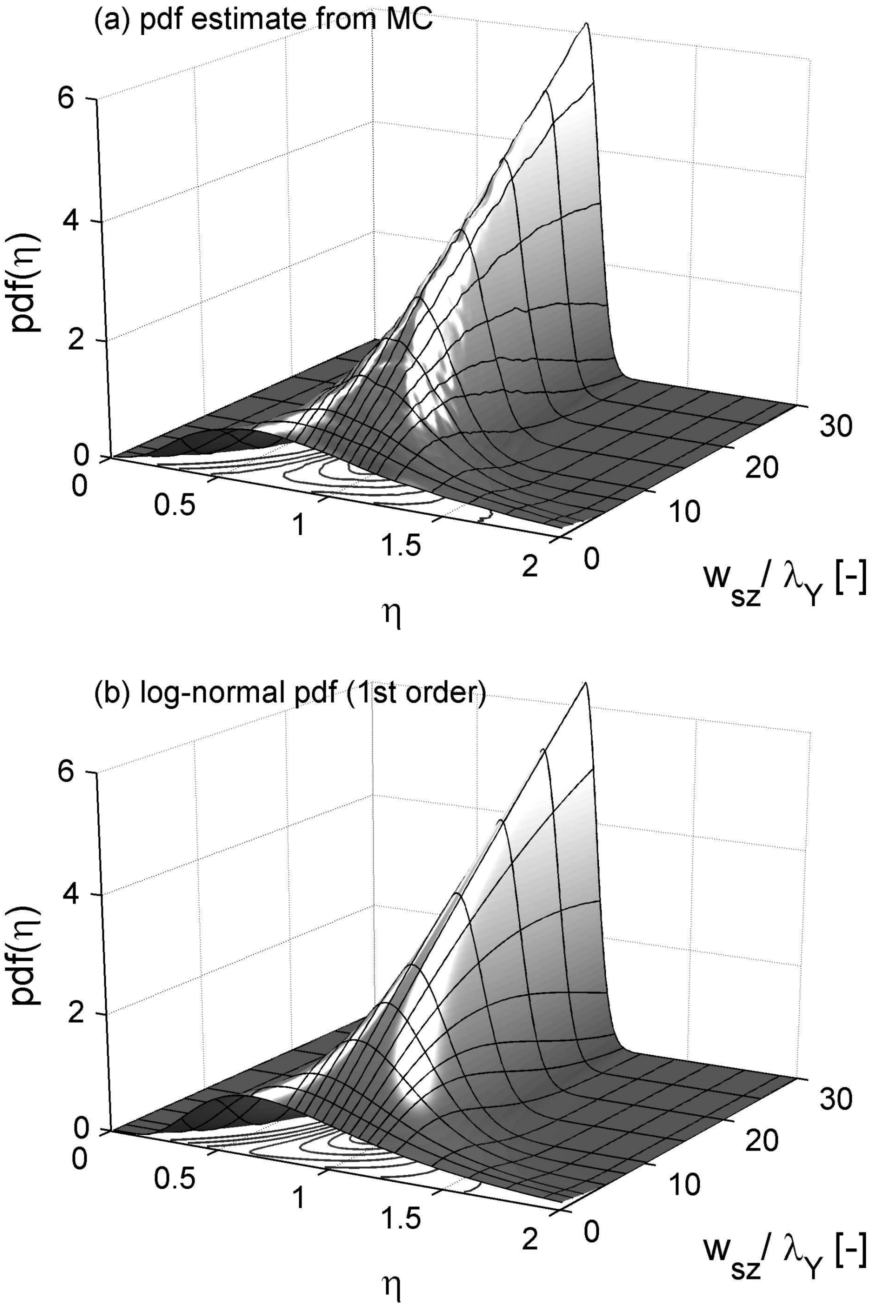

Figure 4: Probability density of source efficiency η and its dependency on geometric source width w_{sz}: (a) estimate from MC analysis with 20,000 realizations and (b) log-normal PDF fitted to the first-order expressions of the mean and variance. The high-valued distribution tail for small w_{sz}/λ is cut-off for better visibility of the overall behavior. For parameter values, refer to Table 1.

Further manipulation of Equation (11) and inserting $x \equiv L_P$ leads to the expression found in Rahman et al. (2005), who substituted the source width with the injection rate divided by ambient flow. Adapted for our work, the expression given in Rahman et al. (2005) reads:

$$L_P \quad = \quad \frac{U}{D_{22}} \left[\frac{\eta \, \mathrm{w_{sz}}}{4 \, \mathrm{erf}^{-1} \left(\frac{\mathrm{c}}{\mathrm{c_o}} \right)} \right]^2 . \tag{12}$$

The above result shows, theoretically, the quadratic law between L_P and η for the physical case analyzed in this work (with a slope equal to 2 when applying the logarithm). As for the statistical distribution of L_P, Monte-Carlo results again suggest a skewed distribution (not shown here), which is confirmed by the scaling with η^2 in Equation (12). In fact, one may re-write the above equation as $L_p = A\eta^2$ where A accounts for all the other parameters present in Equation (12). By transformation of variables, we can obtain a PDF f_L for L_p from the assumed log-normal PDF f_η of source efficiency η with our analytical first-order moments (see Section 3.3):

$$f_L(L_p) = \frac{1}{2\sqrt{AL_p}} f_\eta(\sqrt{L_p/A}). \tag{13}$$

Figure 6 displays the comparison between Equation (13) and the empirical PDF of L_p obtained from numerical Monte Carlo simulations for c/c_o= 0.2. The Monte Carlo results show a larger variance of L_p because effective source width is not the only source of uncertainty.

Equation (12) also implies that the significance of η as a explanatory variable for L_P vanishes with increasing w_{sz}, because its variance decreases with w_{sz} as indicated by equation (12) and other sources of uncertainty downstream of the source start to dominate.

4.2. Plume Spatial Moments

Here, we quantify some of the aspects observed in Figures 1 and 2. Figures 7.a-b shows how the spatial moments of the plume depend on the source efficiency under the parameter values provided in Table 1. Results are obtained through numerical Monte-Carlo simulations. Here, we analyze the mass flux $m_{o,flux}$, relative transversal dispersivity $\alpha_{t,eff}$ and the macroscopic

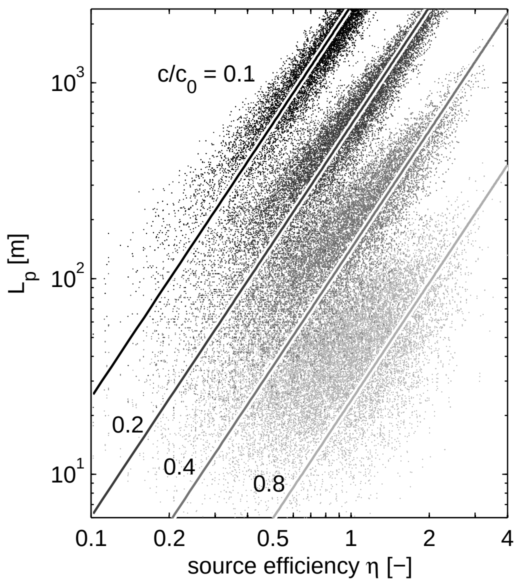

Figure 5: Plume length (L_P) versus source efficiency obtained through numerical Monte Carlo simulations. Results conditional on c/c_o= 0.1, 0.2, 0.3 and 0.5 with simulation parameter values in Table 1.

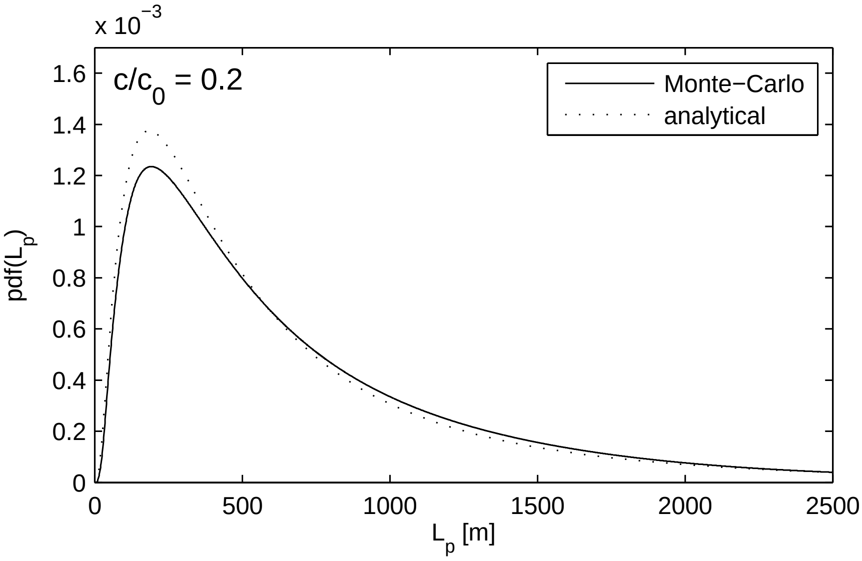

Figure 6: Probability density function for plume length (L_P). Comparison between analytical solution (Eq. 13) and numerical Monte Carlo simulation. Results for c/c_o= 0.2 with simulation parameter values in Table 1.

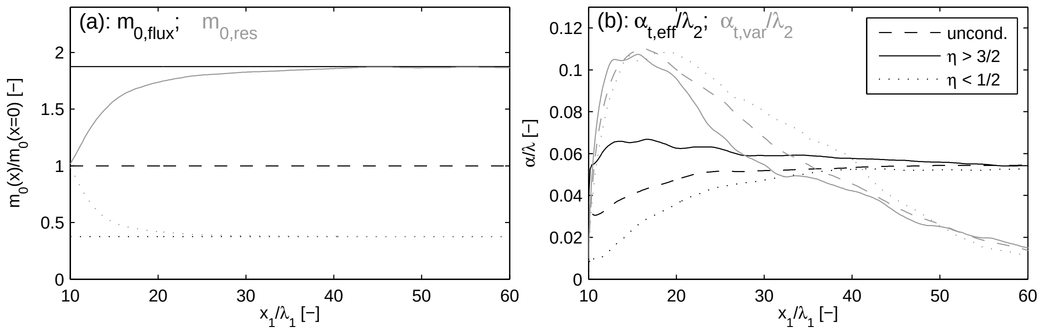

Figure 7: Plume spatial moments (conditional and unconditional) as a function of the normalized longitudinal distance x_1/λ_1. Dashed curve denotes unconditional simulations. Pointed and solid curves corresponds to simulations conditioned on $\eta > 3/2$ and $\eta < 1/2$. Notice that in the current scenario we have $\lambda_1 = \lambda_2 = \lambda$. For parameter values, refer to Table 1.

transversal dispersivity $\alpha_{t,var}$ of meandering. The later is solely due to the variance of the transverse centroid position of the plume, i.e., it quantifies meandering. The sum of $\alpha_{t,eff}$ and $\alpha_{t,var}$ yields the classical macrodispersivity. The following equations were used to estimate the above-mentioned quantities:

$$\begin{aligned} m_{o,flux}(x_1) &= \int_A [\mathbf{q}(\mathbf{x})c(\mathbf{x})]\cdot \mathbf{n}dA; && (14)\\ \alpha_{t,eff}(x_1) &= \frac{1}{2Um_{o,res}}\frac{\partial}{\partial x_1}[\langle m_{22,c}(x_1)\rangle]; && (15)\\ \alpha_{t,var}(x_1) &= \frac{1}{2Um_{o,res}}\frac{\partial}{\partial x_1}[\langle m_2(x_1)\rangle], && (16)\end{aligned}$$

where $m_{22,c}$ denotes the second central spatial moment (around individual plume centroids in individual realizations), $m_2/m_{o,res}$ is the plume's centroid position in x_2, and $m_{o,res}$ is the total resident mass integrated over x_2 (Rubin, 2003). U is the mean velocity in the longitudinal direction and A is the cross-sectional area.

For Figure 7.a, we observe how the amount of resident mass (at the cross section of the domain perpendicular to the mean flow direction) increases with travel distance for $\eta > 3/2$. This is due to divergence of streamlines after the source location, leading to a wider plume on average. Evidentely, the opposite occurs when streamlines converge ($\eta < 1/2$) after the source zone (see eq. 6). The constant curves in Figure 7.a display the mass flux throughout the longitudinal distance.

Figure 7.b displays some characteristics of the dispersive behavior of the plume conditional (and unconditional) on the flow regime at the contaminant source. For instance, Figure 7.b depicts the plume's relative transversal dispersivity $\alpha_{t,eff}$ (see Andricevic and Cvetkovic, 1998), or *effective dispersion* as termed in Dentz et al. (2000). The curves account for the plume spread without meandering, while the remaining curves for $\alpha_{t,var}$ represent the macroscopic tranversal dipersion due to the sole variance of the plume's transversal centroid position. For $\eta > 3/2$, the focusing of streamlines at the source lead to higher $\alpha_{t,eff}$ since the streamlines are squeezed. For $\eta < 1/2$, $\alpha_{t,eff}$ is less pronounced. As expected, the unconditional curve lies in between the conditional cases. To measure the intensity of plume meandering conditional on η, we refer again to Figure 7.b ($\alpha_{t,var}$ curves): It can be seen that larger η implies wider plumes, thus less prone to the effect of meandering. The opposite behavior is observed for smaller η.

In all plots in Figure 7, a characteristic distance can be observed in which the local effect of conditioning fades away. Eventually, after this characteristic distance, the curves become parallel except for the artifact of Monte-Carlo simulation. However, the global inferred effect on plume statistics prevails for all traval distances.

4.3. Significance

The power of source efficiency as explanatory variable for concentration can be visualized by mapping their Pearson's correlation coefficient $r{=}r[c(\mathbf{x}), \eta]$ throughout the domain. The corresponding map, obtained from our Monte-Carlo transport simulation, is shown in Figure 8. Correlations of η with logconductivity and hydraulic heads are given Figure 8.a-b. The correlation of η with concentration (see Figure 8.c-e) is always positive, because a higher source efficiency leads to a larger total mass flux and wider plume emitted by the source. The correlation is highest, about 0.9, along the plume center line: The effective source width dictates the persistence of high concentrations along the plume's center line, see Figure 5. Correlations of about 0.5 prevail throughout most regions of the plume. Only locations outside the plume fringes show almost no correlation. In those regions, only extreme transverse (secondary) flow effects, not linked to the hydraulic circumstances at the source, can have an effect.

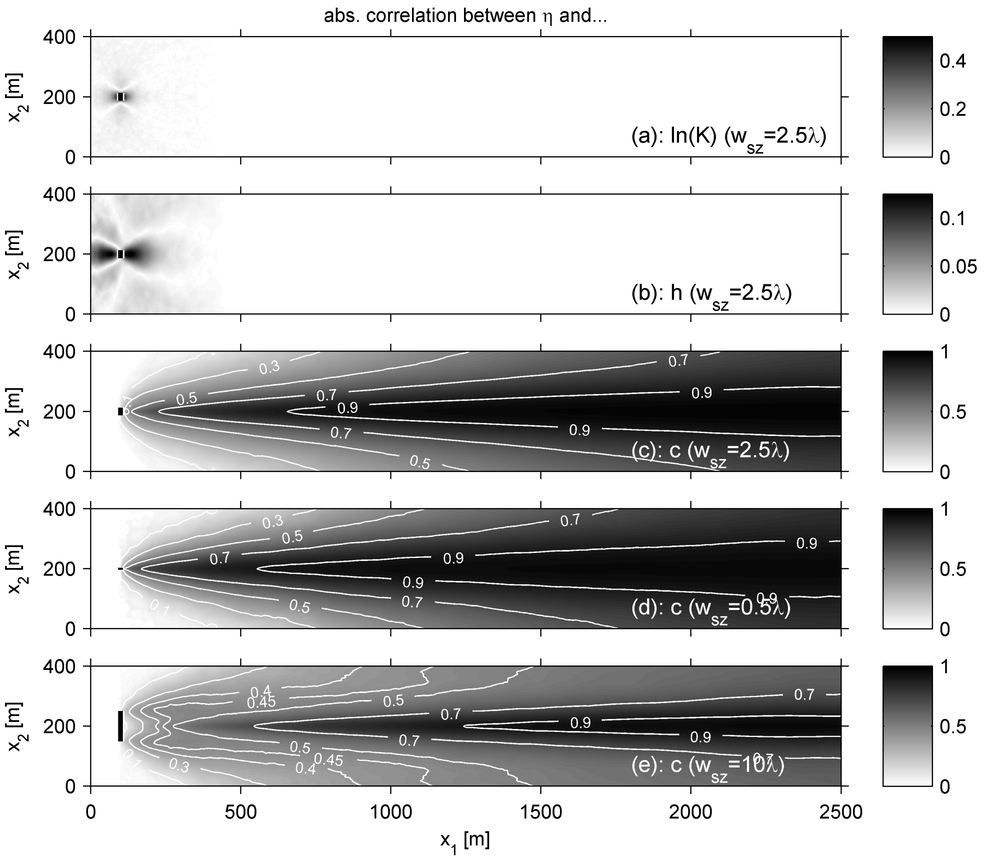

Figure 8: Correlations (absolute values) of (a) $Y = \ln T$, (b) heads and (c)-(e) concentration with source efficiency η. Correlations between η and concentrations are obtained for (c) w_{sz}=2.5 λ, (d) w_{sz}= 0.5 λ, and (e) w_{sz}= 10 λ (as depicted in the plots). Numerical result from Monte-Carlo analysis with 20,000 realizations. For parameter values, refer to Table 1.

The area with high correlation mostly coincides with the area of high expected concentrations, stressing the potential of effective source width to effectively reduce the coefficient of variation of concentration within wide areas of the plume. The fact that source efficiency controls the large-time persistence of peak (high) concentrations along the plume's center line, with high correlations found especially at large distances, unambiguously underlines the surprising importance of near-source sampling for far field prediction shown in Nowak et al. (2010). In addition, Figure 8.c-e illustrates how the correlation map changes according to w_{sz}. Results are plotted for $w_{sz}= 0.5\lambda$, 2.5λ and 10λ. Wider source width leads to a down-gradient shift of the iso-lines present in the correlation map (for instance, see the 0.9 isoline for $w_{sz}= 0.5\lambda$ and $w_{sz}= 10\lambda$). This result is in agreement with the physical insight given in Equation (10), summarized in Figure 3: As w_{sz} increases, thus approaching ergodicity in the sense that the volume average of the specific discharge equals the ensemble average (thus making the total discharge Q_{sz} through the source a deterministic quantity), the explanatory strength of source efficiency for downstream plume characteristics becomes less pronounced. However, its significance prevails for longer travel distances.

4.4. Implications for Site Investigation

Nowak et al. (2010) have identified optimal sampling strategies for minimum variance prediction of contaminant concentrations at an environmentally sensitive location located downgradient of the source. Their results showed that large portion of the samples were located around the source zone and that the uncertainty in plume prediction was reduced by sampling hydraulic conductivities and heads near the source. They hypothesized that the major source of uncertainty addressed by these optimal sampling schemes is the total volumetric water flux passing through the source area. This hypothesis is confirmed theoretically and numerically in the current work.

The correlations depicted in Figure 8.a-b confirm that hydraulic conductivities and head measurements are informative for the effective source width, and hence for far-field prediction. In other words, a small set of measurements (heads and conductivities) located around the source helps to identify the actual value of effective source width and improve prediction power as discussed in the previous sections.

4.5. Alternative Release Conditions

The results shown in this work are under the assumption of a line source with fixed concentration c_o. Relevant physical scenarios leading to the results shown here may be, for example, a fast dissolution process (e.g., of a DNAPL contamination with finely dispersed residual saturation) that installs solubility limit. However, other scenarios can occur such as: (I) Fixed mass flux release of a contaminant (e.g., a leaking tank with instance dissolution) or (II) a slow kinetic dissolution process (e.g., diffusion of remaining contaminant out of low-conductivity regions after an incompleter source remediation).

In both cases, all considerations in plume width and dispersion hold because they are linked to the geometrical characteristics of the contaminant source. Equation (6) can apply, in the re-arranged form $c_f = \dot{m}/Q_{sz}$, to case (I). Here, c_f denotes the flux-averaged concentration determined from a fixed mass flux $\dot{m}$. In this scenario, η will be connected with the uncertainty of the concentration leaving the source since $Q_{sz} = \eta \langle Q_{sz} \rangle$ (see Equation 3). Therefore, in that case, the statistics of concentrations are linked with the statistics of η.

In case (II), the flux-averaged concentration leaving the source will depend on the resident time of water flowing through the source (τ_{sz}). In this case, one may assume $\eta \propto \langle \tau_{sz} \rangle / \tau_{sz}$, where $\langle \tau_{sz} \rangle$ denotes the ensemble expectation of residence time within the source area.

In summary, even under other contaminant and release conditions, similar effects, as discussed in previous sections, will still lead to the same importance of source hydraulics for downstream plume predictions.

5. Summary of Conclusions

In this paper, we have shown that better understanding of the flow regime through the source zone can provide better contaminant predictions. We formally introduced the concept of the effective source width w_{eff} and source efficiency η, and we illustrated and analyzed how knowledge of these quantities can better help quantify contaminant transport. We define the effective source width via the actual, rather than the expected, hydraulic flux through the source area and source efficiency as a factor that absorbs all randomness of the effective source width. In the current work, we highlight the following points:

1. An analytical solution for the statistics of η was formally derived up to first-order. The solution was succesfully compared with numerical

Monte-Carlo simulations. We showed how the variance of η decreases with the geometrical source width and reaches ergodicity when w_{sz} is equal to approximately 100 transversal integral scales. The obtained closed-form solution proved robust for values of σ_Y^2 far above unity.

2. The PDF shape for η was computed numerically and we showed that it can reasonably well approximated by a log-normal distribution.
3. It was shown that (and how) source zone release conditions impact the concentration mean and variance fields. In particular attention, we point out its role in defining the bimodal behavior of the concentration variance with strong implications in risk assessment.
4. The relationship between η and plume length L_P was also addressed. For the physical scenario analyzed, L_P scales with η^2. Therefore, effective source width can be used to better predict the extent of contamination at a prescribed concentration level within the field. This shows how η can be used in applications that are of interest in risk assessment, for example, determining maximum contaminant levels (MCL) or for driving sampling campaigns within a health risk-driven approach as highlighted in de Barros and Rubin (2008) and de Barros et al. (2009).
5. The impact of conditioning plume spatial moments on source characteristics is also investigated. We quantified how both mass fluxes and relative dispersion increases and centroid variance descreases with increasing source efficiency η.

In summary, local hydraulic conditions in the area of contaminant release have a strong impact on plume characteristics. As shown throughout this work, knowing the hydraulics near the contaminant source is of high importance even for far-field predictions of contaminant transport, e.g., when dealing with practical problems, such as estimating human health risk due to groundwater contamination. Moreover, the current paper provides a simple approach to increase the predictive power of existing analytical solutions. As an outlook of future work, the analytical solution, as well as the results given here, could be particularly useful to quantify the additional dilution effects due to inclusions of high- (or low-) permeability materials at later travel distances. This would help to theoretically underline the results published by Rolle et al. (2009), where the impact of inclusions on dilution of contaminants was shown experimentally.

Acknowledgments

The authors would like to thank the German Research Foundation (DFG) for financial support of the project within the Cluster of Excellence in Simulation Technology (EXC 310/1) at the University of Stuttgart. We also wish to thank the reviewers for constructive comments. We acknowledge Marco Dentz for his comments and suggesting the analysis performed in Figure 6.

Appendix A. Flow and Transport Formulation

In our illustrations, we limit the solute transport problem to a steady-state continuous line source in a depth-integrated, divergence-free 2D, groundwater flow at steady-state within a domain $\Omega = L \times W$ (length $\times$ width, respectively). The domain boundary $\partial\Omega$ is divided into two parts: $\partial\Omega_i$ with prescribed head $\hat{h}$ and the remaining parts $\partial\Omega \setminus \partial\Omega_i$ with prescribed flux $(\hat{q})$:

$$\begin{aligned} \nabla \cdot \left[T\left(\mathbf{x}\right) \nabla h \right] &= 0\,,\ \forall \mathbf{x} \in \Omega \\ h &= \hat{h} \quad ,\forall \mathbf{x} \in \partial\Omega_i \\ -\mathbf{n} \cdot \left[T\left(\mathbf{x}\right) \nabla h \right] &= \hat{q} \quad ,\forall \mathbf{x} \in \partial\Omega \setminus \partial\Omega_i, \end{aligned} \tag{A.1}$$

where $T\left(\mathbf{x}\right)\left[L^2/t\right]$ is the locally isotropic, spatially heterogeneous transmissivity and $h\left[L\right]$ is hydraulic head. We can relate each component of the the Darcy flux $\mathbf{q}\left[L/t\right]$ with the stream function by using the following expressions (Batchelor, 2000; Bear, 1972):

$$\begin{aligned} q_1 &= -\frac{\partial \psi}{\partial x_2} \\ q_2 &= \frac{\partial \psi}{\partial x_1}, \end{aligned} \tag{A.2}$$

where isolines of stream functions and hydraulic heads are always orthogonal to each other, forming a potential flow net, in absence of sources and sinks.

The corresponding governing equation for the stream function ψ and boundary conditions are given as (Bear, 1972):

$$\begin{aligned} \nabla \cdot \left[\frac{1}{T} \nabla \psi \right] &= 0,\ \forall \mathbf{x} \in \Omega \\ \mathbf{n} \cdot \nabla \psi &= 0 \quad ,\forall \mathbf{x} \in \partial\Omega_i \\ \psi &= \hat{\psi} \quad ,\forall \mathbf{x} \in \partial\Omega \setminus \partial\Omega_i, \end{aligned} \tag{A.3}$$

with $\hat{\psi}$ being a boundary fixed value for the stream function (determined by integration over $\hat{q}$). Steady-state concentration is given by:

$$\mathbf{v} \cdot \nabla c - \nabla \cdot (\mathbf{D}_d \nabla c) = 0, \; \forall \, \mathbf{x} \in \Omega \,, \tag{A.4}$$

where $c\,[M/L^3]$ is concentration, $\mathbf{v} = \mathbf{q}/n_e\ [L/t]$ is velocity, $n_e\,[-]$ is porosity, and $\mathbf{D}_d\,[L^2/t]$ is the local-scale dispersion tensor. Uncontaminated groundwater with $c = 0$ enters at $x_1 = 0$, and the outflow boundary at $x_1 = L$ is unrestricted. The lateral boundaries are closed. We solved these equations using the same numerical implementation as in Nowak et al. (2008).

Appendix B. Relation between Stream Function Statistics and Head Statistics

In order to derive the stream function statistics, we make use of the head correlation structure expressed here in terms of the head variogram Γ_h. A first-order approximation to Γ_h has been provided by Dagan (1985b, 1989). Assumptions in the derivation were unbounded domain, mildly heterogeneous porous media, absence of sources and sinks, and geostatistical stationarity. Much less attention has been given to stream function statistics with a few exceptions such as Cirpka et al. (2004), who used linear error propagation and adjoint-state sensitivities to obtain the variance of stream function differences in the hydraulic design of a funnel-and-gate system.

Our starting point is equation (A.3), which is formally identical to the groundwater flow equation. To obtain the stream function variogram, we follow the same formal steps taken by Dagan (1985b) for the head variogram and provided in more detail in Dagan (1989) and Rubin (2003). Let $Y = \ln T$ such that $Y(\mathbf{x}) = \langle Y \rangle + Y'(\mathbf{x})$. Substituting these expressions in equation (A.3) and using $1/T = \exp(-Y) = \exp(-Y')/T_G$, we have:

$$\begin{aligned} \nabla \cdot \left[e^{-\langle Y \rangle} e^{-Y'} \nabla \psi \right] &= 0; \\ \Leftrightarrow \nabla^2 \psi - \nabla \psi \cdot \nabla Y' &= 0. \end{aligned} \tag{B.1}$$

By expanding the stream function into a polynomial of conductivity fluctuations Y', we obtain:

$$\nabla^2(\psi_o + \psi_1 + \ldots) - \nabla(\psi_o + \psi_1 + \ldots) \cdot \nabla Y' = 0. \tag{B.2}$$

Solving the equation for each *order* separately yields:

$$\begin{aligned}(n=0):&\quad \nabla^2\psi_o = 0;\\ (n=1):&\quad \nabla^2\psi_1 = \nabla\psi_o\cdot\nabla Y',\end{aligned}\tag{B.3}$$

where the solution of $(n = 0)$ for uniform-in-the-average flow must satisfy:

$$-\frac{\partial\psi_o}{\partial x_i} = \gamma_i\,. \tag{B.4}$$

Due to their orthogonality (see Batchelor, 2000), heads and stream functions are coupled as:

$$\begin{aligned}-T_G\frac{\partial h}{\partial x_1} &= \frac{\partial\psi}{\partial x_2} = -\gamma_2;\\ -T_G\frac{\partial h}{\partial x_2} &= -\frac{\partial\psi}{\partial x_1} = \gamma_1,\end{aligned}\tag{B.5}$$

which implies:

$$\begin{aligned}\gamma_1 &= J_2T_G\\ \gamma_2 &= -J_1T_G\\ \gamma &= \sqrt{\gamma_1^2+\gamma_2^2} = T_GJ\,,\end{aligned}\tag{B.6}$$

with $J = \sqrt{J_1^2 + J_2^2}$. There are two differences between the stream function formulation and the pressure head formulation: (1) comparing the right-hand side in equation (B.3) for $n = 1$ to Equation 3d of Dagan (1985b), we observe that they have opposite signs due to the appearance of T^{-1} in the stream function equation; and (2) the solution for $n = 0$ contains a gradient of γ_i instead of J_i. Now we duplicate the first-order equation $(n = 1)$ for space coordinates $\mathbf{x}$ and $\mathbf{y}$. Multiplying these two equations leads to:

$$\nabla_x^2\nabla_y^2\psi_1(\mathbf{x})\psi_1(\mathbf{y}) = \sum_{i=1}^{d}\sum_{j=1}^{d}\gamma_i\gamma_j\frac{\partial Y'(\mathbf{x})}{\partial x_i}\frac{\partial Y'(\mathbf{y})}{\partial y_j}\,, \tag{B.7}$$

where d is the physical dimension. Taking the expected value yields the generating equation for the stream function covariance:

$$\nabla_x^2 \nabla_y^2 C_\psi(\mathbf{x}, \mathbf{y}) = \sum_{i=1}^{d} \sum_{j=1}^{d} \gamma_i \gamma_j \frac{\partial}{\partial x_i} \frac{\partial}{\partial y_j} C_Y(\mathbf{x}, \mathbf{y}) \ . \tag{B.8}$$

The opposite sign has vanished now and the generating equation is identical to that for the head covariance, except that $\gamma_i \neq J_i$. This allows to use the analytical solutions derived for the head variogram with substituted coefficients (γ_i), thus leading to a rotation by ninety degrees and scaling by T_G^2.

For the isotropic exponential covariance model, $C_Y(\mathbf{r}) = \sigma_Y^2 \exp[\mathbf{r}/\lambda]$ with variance σ_Y^2 and correlation length λ, the first-order head variogram for lag distances r along the mean flow direction is (see Dagan, 1985b):

$$\Gamma_h(r, 0) = \sigma_Y^2 \lambda^2 J^2 \frac{1}{2} \zeta(r), \tag{B.9}$$

with:

$$\zeta(r) = \frac{1}{2} + \frac{e^{-r/\lambda}\left[\left(\frac{r}{\lambda}\right)^2 + 3\left(\frac{r}{\lambda}\right) + 3\right] - 3}{\left(\frac{r}{\lambda}\right)^2} - Ei\left(-\frac{r}{\lambda}\right) + \left(\frac{r}{\lambda}\right) + e^{-r/\lambda} - 0.4228. \tag{B.10}$$

Due to rotation and scaling, we arrive at the stream function variogram for transverse lag distances as:

$$\Gamma_\psi(0, r) \ = \ T_G^2 \Gamma_h = \sigma_Y^2 \lambda^2 J^2 T_G^2 \frac{1}{2} \zeta(r). \tag{B.11}$$

In summary, the required assumptions necessary for the derivation of equation (9) are: (i) unbounded domain, (ii) uniform-in-the-average steady-state flow, (iii) mildly heterogeneous porous media ($\sigma_Y^2 \lesssim 1$) with absence of sources and sinks, (iv) 2D depth-averaged, and (iv) statistical stationarity.

References

Andricevic, R., Cvetkovic, V., 1998. Relative dispersion for solute flux in aquifers. Journal of Fluid Mechanics 361, 145–174.

Batchelor, G., 2000. An introduction to fluid dynamics. Cambridge Univ Press.

Bear, J., 1972. Dynamics of Fluids in Porous Media. Elsevier Science, New York.

Bellin, A., Salandin, P., Rinaldo, A., 1992. Simulation of dispersion in heterogeneous porous formations: Statistics, first-order theories, convergence of computations. Water Resour. Res. 28, 2211–2227.

Cirpka, O.A., Bürger, C.M., Nowak, W., Finkel, M., 2004. Uncertainty and data worth analysis for the hydraulic design of funnel-and-gate systems in heterogeneous aquifers. Water Resour. Res. 40, doi:10.1029/2004WR003352.

Dagan, G., 1985a. A note on higher-order corrections of the head covariances in steady aquifer flow. Water Resour. Res. 21, 573–578.

Dagan, G., 1985b. Stochastic modeling of groundwater flow by unconditional and conditional probabilities. The inverse problem. Water Resour. Res. 21, 65–72.

Dagan, G., 1988. Time-dependent macrodispersion for solute transport in anisotropic heterogeneous aquifers. Water Resour. Res. 24, 1491–1500.

Dagan, G., 1989. Flow and Transport in Porous Formations. Springer Verlag, Berlin.

de Barros, F.P.J., Rubin, Y., 2008. A risk-driven approach for subsurface site characterization. Water Resour. Res. 44, doi:10.1029/2007WR006081.

de Barros, F.P.J., Rubin, Y., Maxwell, R., 2009. The concept of comparative information yield curves and its application to risk-based site characterization. Water Resour. Res. 45, doi:10.1029/2008WR007324.

Dentz, M., Bolster, D., Le Borgne, T., 2009a. Concentration statistics for transport in random media. Physical Review E 80, 10101.

Dentz, M., Carrera, J., Bolster, D., Le Borgne, T., 2009b. Multipoint concentration statistics for transport in stratified random velocity fields. Physical Review E 80, 36306.

Dentz, M., Kinzelbach, H., Attinger, S., Kinzelbach, W., 2000. Temporal behaviour of a solute cloud in a heterogeneous porous medium. 2. Spatially extended injection. Water Resour. Res. 36, 3605–3614.

Domenico, P., Palciauskas, V., 1982. Alternative boundaries in solid waste management. Ground Water 20, 303–311.

Englert, A., Vanderborght, J., Vereecken, H., 2006. Prediction of velocity statistics in three-dimensional multi-Gaussian hydraulic conductivity fields. Water Resour. Res. 42, doi:10.1029/2005WR004014.

Fiori, A., Dagan, G., 2000. Concentration fluctuations in aquifer transport: A rigorous first-order solution and applications. J. Contam. Hydrol. 45, 139–163.

Fiorotto, V., Caroni, E., 2002. Solute concentration statistics in heterogeneous aquifers for finite Péclet values. Transport in Porous Media 48, 331–351.

Frind, E., Molson, J., Schirmer, M., Guiguer, N., 1999. Dissolution and mass transfer of multiple organics under field conditions: The Borden emplaced source. Water Resources Research 35, 683–694.

Gelhar, L.W., Axness, C.L., 1983. Three-dimensional stochastic analysis of macrodispersion in aquifers. Water Resour. Res. 19, 161–180.

Jaynes, E., 1982. On the rationale of maximum-entropy methods. Proc. IEEE 70, 939–952.

Kapoor, V., Kitanidis, P., 1997. Advection-diffusion in spatially random flows: Formulation of concentration covariance. Stochastic Environmental Research and Risk Assessment (SERRA) 11, 397–422.

Nowak, W., de Barros, F.P.J., Rubin, Y., 2010. Bayesian geostatistical design: Task-driven optimal site investigation when geostatistical model is uncertain. Water Resources Research 46, doi:10.1029/2009WR008312.

Nowak, W., Schwede, R.L., Cirpka, O.A., Neuweiler, I., 2008. Probability density functions of hydraulic head and velocity in three-dimensional heterogeneous porous media. Water Resour. Res. 44, doi:10.1029/2007WR006383.

Parzen, E., 1962. On estimation of a probability density function and mode. The annals of mathematical statistics 33, 1065–1076.

Rahman, M., Jose, S., Nowak, W., Cirpka, O., 2005. Experiments on vertical transverse mixing in a large-scale heterogeneous model aquifer. Journal of contaminant hydrology 80, 130–148.

Rolle, M., Eberhardt, C., Chiogna, G., Cirpka, O.A., Grathwohl, P., 2009. Enhancement of dilution and transverse reactive mixing in porous media: Experiments and model-based interpretation. Journal of contaminant hydrology In Press.

Rubin, Y., 1991. Transport in heterogeneous porous media: Prediction and uncertainty. Water Resour. Res 27, 1723–1738.

Rubin, Y., 2003. Applied Stochastic Hydrogeology. Oxford University Press, Oxford.

Rubin, Y., Cushey, M.A., Bellin, A., 1994. Modeling of transport in groundwater for environmental risk assessment. Stochastic Hydrol. Hydraul. 8, 57–77.

Rubin, Y., Sun, A., Maxwell, R., Bellin, A., 1999. The concept of block-effective macrodispersivity and a unified approach for grid-scale- and plume-scale-dependent transport. J. Fluid Mech. 395, 161–180.

Schwede, R.L., Cirpka, O.A., Nowak, W., Neuweiler, I., 2008. Impact of sampling volume on the probability density function of steady state concentration. Water Resour. Res. 44, doi:10.1029/2007WR006668.

Singh, V., 1997. The use of entropy in hydrology and water resources. Hydrological Processes 11, 587–626.

Valocchi, A.J., Nakshatrala, K., 2009. Reactions along Transverse Mixing Zones in Heterogeneous Aquifers: Using Effective Dispersion Coefficients and Multi-Scale Finite Element Methods . Eos Trans. AGU Abstract Number H32C-04 90(52).

Wasserman, L., 2004. All of statistics: a concise course in statistical inference. Springer Verlag.

Werth, C., Cirpka, O., Grathwohl, P., 2006. Enhanced mixing and reaction through flow focusing in heterogeneous porous media. Water Resources Research 42, W12414.